Void-induced dissolution in molecular dynamics simulations of NaCl and water

Ranjit Bahadur and Lynn M. Russell[a)]
Scripps Institution of Oceanography, University of California-San Diego, La Jolla, California 92093-0221

Saman Alavi
Steacie Institute for Molecular Sciences, National Research Council of Canada, Ottawa, Ontario K1A 0R6, Canada

Scot T. Martin
Division of Engineering and Applied Sciences, Harvard University, Cambridge, Massachusetts 02138

Peter R. Buseck
Department of Geological Sciences, Arizona State University, Tempe, Arizona 85287 and Department of Chemistry/Biochemistry, Arizona State University, Tempe, Arizona 85287

(Received 30 December 2005; accepted 14 February 2006)

To gain a better understanding of the interaction of water and NaCl at the surface during dissolution, we have used molecular dynamics to simulate the interface with two equal-sized slabs of solid NaCl and liquid water in contact. The introduction of voids in the bulk of the salt, as well as steps or pits on the surface of the NaCl slab results in a qualitative change of system structure, as defined by radial distribution functions (RDFs). As an example, the characteristic Na–Na RDF for the system changes from regularly spaced narrow peaks (corresponding to an ordered crystalline structure), to a broad primary and smaller secondary peak (corresponding to a disordered structure). The change is observed at computationally short time scales of 100 ps, in contrast with a much longer time scale of 1 μs expected for complete mixing in the absence of defects. The void fraction (which combines both bulk and surface defects) required to trigger dissolution varies between 15%–20% at 300 K and 1 atm, and has distinct characteristics for the physical breakdown of the crystal lattice. The void fraction required decreases with temperature. Sensitivity studies show a strong dependence of the critical void fraction on the quantity and distribution of voids on the surface, with systems containing a balanced number of surface defects and a rough surface showing a maximum tendency to dissolve. There is a moderate dependence on temperature, with a 5% decrease in required void fraction with a 100 K increase in temperature, and a weak dependance on water potential model used, with the SPC, SPC/E, TIP4P, and RPOL models giving qualitatively identical results. The results were insensitive to the total quantity of water available for dissolution and the duration of the simulation. © *2006 American Institute of Physics*. [DOI: 10.1063/1.2185091]

I. INTRODUCTION

The interactions of water and salt are important both environmentally[1] and technologically.[2] Interfaces between sodium chloride and water or solution play an important role in atmospheric chemistry. Sodium chloride is the major constituent of atmospheric sea salt particles. Such particles exist as crystals, either covered with water or an aqueous solution,[3] rather than an anhydrous phase. The water layer can alter reactions of the NaCl surface with pollutants such as nitrous gases or nitric acid.[4–7] These particles are also a dominant source of reactive atmospheric chlorine compounds that affect the ozone balance and oxidize organic substances.[8,9] Aqueous sodium chloride solutions in contact with crystalline NaCl surfaces are an example of aqueous electrolytes in contact with a salt interface. The surface behavior of alkali halides in contact with saturated solutions plays an important role in the characterization of processes such as corrosion, tertiary oil recovery, and crystallization. The industrial process of floatation, which is used to recover approximately 80% of all potassium minerals, is dependent on surface alkali halide interactions with aqueous media.

Dissolution and crystal growth from a solution are phase transitions corresponding to the disappearance and formation of an ordered phase, respectively, for a two component mixture of NaCl and water. Though these processes are well described from a macroscopic thermodynamic point of view, little knowledge is available at the level of molecular interactions.[10–12] Molecular dynamics simulations may provide insight on microscopic behavior, which is of particular interest for nanoparticles.

Sodium chloride solutions as well as the crystalline phase have been widely studied using simulation techniques.[13–17] In addition to simulation of bulk phases, the dissolution properties of single ions in small water clusters have also been studied.[18,19] More recently, studies have focused on the interface of solid NaCl and water[20,21] and on NaCl in contact with a supersaturated solution.[22] With the

[a)]Electronic mail: lmrussell@ucsd.edu

longest computationally reasonable simulation runs, only limited interaction was observed between the liquid and solid phases because the time scales of dissolution and crystallization are expected to drastically exceed the scope of direct simulation. There are therefore few simulation studies available on the kinetic process of dissolution.[23]

Computational studies of calcite dissolution[24,25] have shown that the highest probability of dissolution is not at flat crystalline faces but at the edges of steps and kinks which are naturally present on most crystalline surfaces.[26] These simulations are supported by experimental studies of microscopic dissolution at mineral surfaces.[27,28] Recently, the introduction of voids into the crystal structure has been observed to initiate melting in computational studies,[29,30] which is a temperature-driven loss of structure analogous to dissolution. In this work, we use molecular dynamics to combine these approaches and initiate dissolution at the NaCl-water interface by introducing defects to the crystal surface and in the crystal volume.

We present a study of the onset of dissolution. Section II describes the molecular dynamics methods used, Sec. III outlines the underlying thermodynamic considerations, Sec. IV presents the predicted dissolution behavior, and Sec. V summarizes several sensitivity studies.

II. METHOD AND CALCULATIONS

A. Force fields

A key input in classical molecular dynamics simulations is the intermolecular potential. Most widely used models include two-body short-range repulsion and attraction between spherical sites, together with electrostatic interactions.

The ion-ion interactions are modeled using a Born-Huggins-Mayer potential,[31]

$$V(r_{ij}) = \frac{e^2 q_i q_j}{r_{ij}} + A_{ij}\exp(-r_{ij}/\rho_{ij}) - \frac{C_{ij}}{r_{ij}^6} - \frac{D_{ij}}{r_{ij}^8}, \quad (1)$$

where V is the interaction potential, r_{ij} is the separation between ions i and j, eq_i and eq_j are the scaled atomic charges, and A_{ij}, ρ_{ij}, C_{ij}, and D_{ij} are parameters specific to each ion pair interaction. The form of the potential as written contains both attractive and repulsive terms.

The description of water molecules in molecular dynamics (MD) is less straightforward, with a wide variety of potentials available. In our work, we use four contrasting descriptions of the water molecule. Our intention is not to present a comparison of these models, but to assess the degree to which our technique depends on the chosen water model. The SPC model[32] has been used extensively in simulation studies of thermodynamic and transport properties of ions and uncharged solutes. In this model, the OH bond distance is constrained at 1 Å and the angle between the two OH bonds is fixed at 109.47°. Partial charges are placed on the oxygen and hydrogen atoms. The intermolecular interaction between a pair of water molecules is

TABLE I. Born-Huggins-Mayer (BHM) potential parameters (Ref. 37) for Na and Cl used in Eq. (1).

Ion-ion	A (kJ mol^{-1})	ρ (Å)	C (kJ mol^{-1} Å^6)	D (kJ mol^{-1} Å^8)
Na–Na	40 872.1	0.312	101.2	48.2
Cl–Cl	33 628.7	0.318	6981.5	13 429.1
Na–Cl	121 081.4	0.318	674.5	837.1

$$V(r_{ij}) = \frac{e^2 q_i q_j}{r_{ij}} + \epsilon_{ij}\left(\left(\frac{\sigma_{ij}}{r_{ij}}\right)^{12} - \left(\frac{\sigma_{ij}}{r_{ij}}\right)^{6}\right), \quad (2)$$

where ϵ_{ij} and σ_{ij} are Lennard-Jones-type interaction parameters and the indices sum over the various force centers in the water molecule.

The SPC/E model[33] extends the SPC model by modifying the values of the partial charges to better account for the measured dipole moment of the water molecule. The TIP4P potential model[34] provides a further improvement over the SPC/E model in describing the polar nature of the water molecule. This model has an additional charge center with a fixed negative charge placed on the bisector of the HOH angle, with fixed charges on the hydrogen atoms. The internal structure of water is considered to be rigid, with the OH bond lengths constrained at 0.9572 Å, the HOH bond angle at 104.52°, and a separation of 0.15 Å between the oxygen atom and charge center. The form of the intermolecular potential is the same as Eq. (2), with the summation now over four force centers. The polarization of the hydrogen and oxygen atoms is dealt with explicitly in the RPOL (Ref. 35) three point model.

Ion-water interactions are modeled using Lennard-Jones-type interactions.[36] It should be noted that the Lennard-Jones center is placed solely on the oxygen atoms and there are no Lennard-Jones (LJ)-type interactions with either the water hydrogens, or the extra charge center present in the TIP4P model. The values for and sources of the parameters used for the potentials in Eqs. (1) and (2) are listed in Tables I and II.

B. Molecular dynamics

Molecular dynamics simulations have been performed at constant pressure and temperature (*NPT*) on a NaCl supercell consisting of $4\times4\times2$ unit cells in contact with an equal volume of liquid water in DL_POLY version 2.14.[39] The NaCl supercell contains 128 ion pairs and the liquid volume contains 196 water molecules. Recent MD studies show that supercells of this size are sufficient to reproduce solid properties.[40–43]

The *NPT* ensemble simulates physical conditions at which dissolution might be observed. The temperature and pressure were held constant using the Nosé-Hoover

TABLE II. Lennard-Jones parameters (Refs. 36 and 38) used in Eq. (2).

Pair	ϵ (kJ mol^{-1})	σ (Å)
O–O	0.6502	3.166
Na–O	0.5216	2.876
Cl–O	0.5216	3.785

algorithm,[44,45] as implemented in the DL_POLY program. Relaxation times of 0.1 and 2.0 ps were used for the thermostat and barostat, respectively. The equations of motion were integrated using the Verlet leapfrog scheme.[10,46,47] All interatomic interactions between the atoms in the simulation box and the nearest image sites were calculated within a cutoff distance of $R_{\text{cutoff}}=10$ Å for the simulation cell which has initial dimensions of $21.1\times21.1\times21.1$ Å^3. The Coulombic long-range interactions were calculated using Ewald's method,[10,46–48] with a precision of 1×10^{-6}. The thermostat scales the velocities of the atoms in a nonphysical manner but allows the determination of properties from the equilibrated final structures from converged simulations at each temperature. The time step used in the simulations was 0.5 fs. The combined system is allowed to equilibrate for 25 fs (50 000 time steps) before the thermodynamic properties of the resulting mixture were calculated.

C. Simulation setup

The starting configuration for the NaCl ion pairs corresponds to the crystalline unit cell determined by x-ray spectroscopy.[49] A separate simulation is performed using only water molecules, which are allowed to come to equilibrium at 300 K. The final configuration is used as the initial state for the water layer in the combined simulation. At each temperature voids are introduced in the crystalline layer by removing ion pairs in steps of 5% of the total, ranging from 0% (no ion pairs removed) to 40% (52 ion pairs removed). The locations of the voids are differentiated into either "surface voids" corresponding to surface roughness, and "interior voids" corresponding to a combination of macroscopic pores and crystal point defects. The system is then simulated to see if dissolution occurs.

The introduction of too many voids in the NaCl crystal structure is expected to lead to mechanical instability and a breakdown of the lattice by a process different from dissolution. Simulations are also performed on a crystalline slab in the absence of any water at each temperature and void combination in order to locate the point of mechanical instability. The simulation cells are set up with cubic periodic boundary conditions, which result in bulk phases for the unmixed components, and alternating semi-infinite slabs (in the X and Y directions) of NaCl and water in the mixed simulation.

In addition to determining the total void fraction needed to initiate dissolution, the effect of the distribution was also studied. A series of void distribution functions is defined which characterize the nature of voids introduced, keeping the total number of voids constant. The fraction of surface voids introduced is

$$\phi=\frac{n_{\text{surface}}}{n_t}, \tag{3}$$

where n is the number of voids and subscripts "surface" and t (total) indicate their location. The remaining void distribution functions determine the distribution of distinct and contiguous voids. For this purpose, we define a distinct void to consist of all orthogonally contiguous voids in the crystal lattice (nearest neighbors). The void distribution function for the surface is

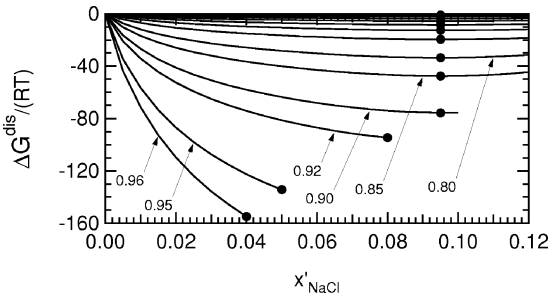

FIG. 1. Scaled values of the free energy change of dissolution from Eq. (8). The mole fraction of NaCl in the solution as defined in Eq. (9) is on the x axis. The different curves correspond to increasing values of the water mole fraction x_{H_2O} as defined in Eq. (10), while keeping the total number of NaCl molecules constant. The curves corresponding to high mole fractions have been labeled using tags, from which the trend of changing mole fraction may be inferred. The curves have all been terminated at the solubility limit of NaCl at this temperature.

$$\phi'=\frac{n_{\text{surface,distinct}}}{n_{\text{surface}}}, \tag{4}$$

where only nearest neighbors on the surface (in two dimensions) are considered. The function characterizes the surface as containing numerous pits ($\phi'=1$) or having few isolated voids that form steps ($\phi'\ll1$). A similar function is defined in three dimensions to characterize the distribution of volume defects between small and large pores.

Simulations of saturated NaCl solutions at various temperatures were used to identify an internally consistent reference phase to illustrate the fully mixed solution for comparison. The size of the simulation cell is identical to the NaCl/water slab simulations, with the number of molecules determined from the bulk density of water and NaCl solubility limit.

III. SOLUTION THERMODYNAMICS

The cubic periodic boundary conditions used in the simulation result in a series of parallel, identical NaCl-water interfaces. We focus on one of these interfaces, which is described by the following equation for the free energy G at constant temperature and pressure, where the subscript s refers to the solid crystalline phase, l to the liquid water phase, and sl to the solid-liquid interface:

$$G^{\text{i}}=n_s^i\mu_s^i+n_l^i\mu_l^i+A_{\text{sl}}^i\sigma_{\text{sl}}^i. \tag{5}$$

The number of moles n_s^i and n_l^i and the interfacial area A_{sl}^i are known quantities based upon the setup of the simulation cell. The chemical potentials μ_s^i and μ_l^i correspond to pure components and are equal to the standard state chemical potentials at these conditions, while σ_{sl}^i is the solid-liquid surface tension between NaCl and pure water. Equation (5) in this form represents the free energy corresponding to the initial state (i) of our simulation. For the final state (f) of the simulation, the free energy G can be written as

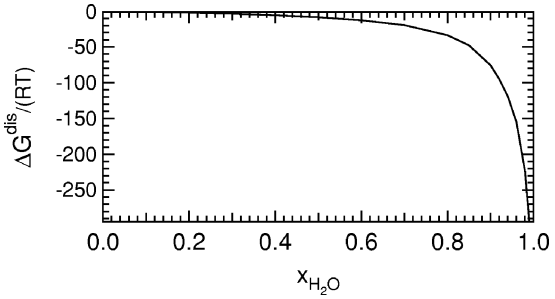

FIG. 2. Scaled value of the free energy change of dissolution from Eq. (8), if the change in surface energy term is negligible. The water mole fraction x axis. The different curves correspond to increasing values of the water mole fraction x_{H_2O} as defined in Eq. (10) is plotted on the x axis. The values were calculated using a constant number of NaCl molecules in the simulation cell and correspond to the most stable states, that is, the minima of the free energy curves in Fig. 1.

$$G^f = n_s^f \mu_s^f + n_l^f (\mu_l^f + RT \ln a_l) + n_i^f (\mu_i^f + RT \ln a_i) + A_{\mathrm{sl}}^f \sigma_{\mathrm{sl}}^f. \tag{6}$$

Equation (6) is perfectly general, because we do not specify *a priori* what the concentration of the aqueous solution phase will be. The additional quantities n_i^f and μ_i^f refer to sodium and chloride ions (if any) which dissolve in the water layer. The quantities a_l and a_i refer to the activities of water and ions in the solution phase, and their logarithms measure the free energy of dissolution, following the treatment in a standard thermodynamics text.[50] The superscripts f and i distinguish the final quantities from their initial values in Eq. (5). The total change in free energy for dissolution can now be calculated as the difference between Eqs. (5) and (6),

$$\Delta G^{\mathrm{dis}} = (n_s^f \mu_s^f + n_i^f \mu_i^f - n_s^i \mu_s^i) + (n_l^f \mu_l^f - n_l^i \mu_l^i) + (A_{\mathrm{sl}}^f \sigma_{\mathrm{sl}}^f - A_{\mathrm{sl}}^i \sigma_{\mathrm{sl}}^i) + RT(n_l^f \ln a_l + n_i^f \ln a_i), \tag{7}$$

where the terms have been grouped for convenient simplification. If we use the same reference state to measure the chemical potentials of all species, then the chemical potentials of the standard states in Eq. (6) are equal to the chemical potentials of the pure species. Also, the total number of both solid and liquid molecules must be conserved. That is,

$$\mu_s^i = \mu_s^f = \mu_i^f,$$

$$\mu_l^i = \mu_l^f,$$

$$n_s^i = n_s^f + n_i^f,$$

$$n_l^i = n_l^f.$$

On substituting these four conditions in Eq. (7), the first two groupings cancel out. Assuming uniform dissolution across the surface, the interface remains flat and the total interfacial area does not change. The value of the solid-liquid surface tension has an experimentally measured value of $\sigma_{\mathrm{sl}} = 29 \pm 20$ mN m^{-1}.[51–53] It is reasonable to assume that any uncertainties of the net change in surface energy due to change in the actual surface tension between NaCl and dilute solution and any smoothing of the surface are small relative to the 20 mN m^{-1} uncertainty in σ_{sl}, such that

$$A_{\mathrm{sl}}^i \sigma_{\mathrm{sl}}^i \approx A_{\mathrm{sl}}^f \sigma_{\mathrm{sl}}^f.$$

Thus, the final grouping of terms in Eq. (7) also cancels out, and we are left with the simplified result

$$\frac{\Delta G^{\mathrm{dis}}}{RT} = n_l \ln a_l + n_i \ln a_i. \tag{8}$$

Numerically calculated values for the free energy change of dissolution have been plotted in Fig. 1, as a function of final solution concentration. The concentration is expressed as the mole fraction of NaCl in the solution phase,

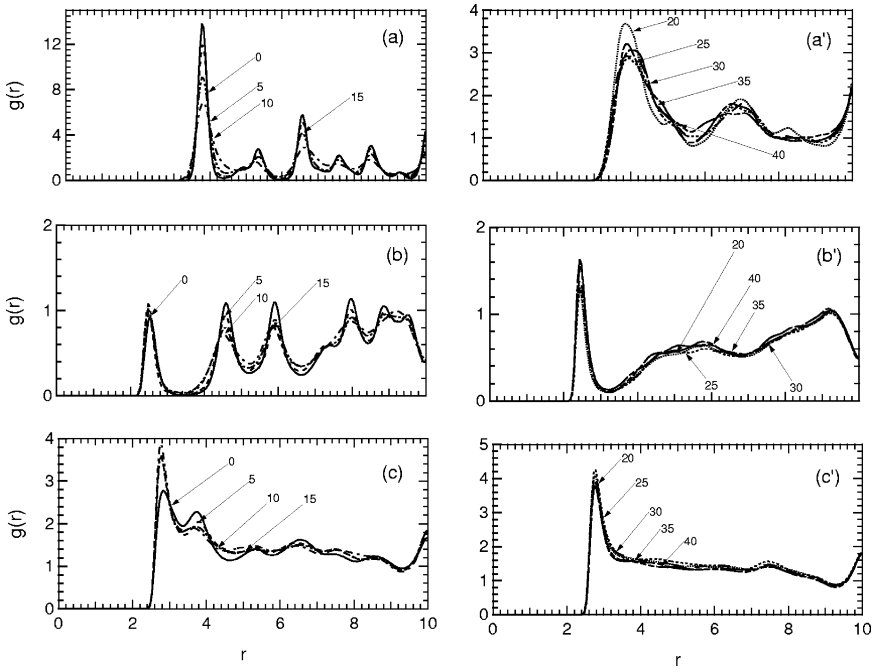

FIG. 3. Comparison of characteristic system RDFs showing a change in morphology when voids are present at 300 K. The x axis is radial distance in angstroms. (a) and (a′) show the two Na–Na RDF families above and below the critical void fraction. (b) and (b′) compare the Na–O, and (c) and (c′) compare the O–O RDFs. An increasing amount of void is indicated across the figures.

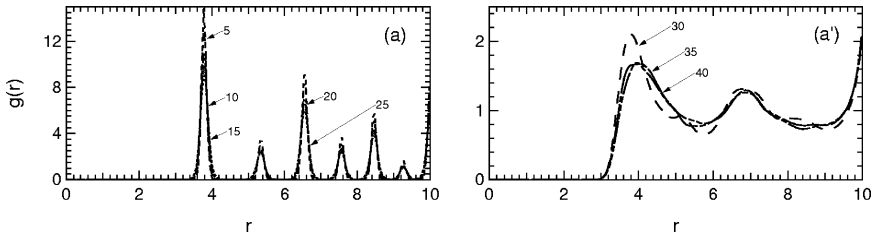

FIG. 4. Na–Na RDFs generated by simulating a NaCl crystalline slab containing voids, but not in contact with water at 300 K. In contrast to the corresponding RDFs illustrated in Figs. 3(a) and 3(a′), the transition occurs at a higher void content of 30%.

$$x'_{\mathrm{NaCl}} = \frac{n_i^f}{n_l^f + n_i^f}. \tag{9}$$

The values were calculated for several possible simulation cells containing different amounts of water. The NaCl/water ratio is expressed as total mole fraction of water,

$$x_{\mathrm{H_2O}} = \frac{n_l}{n_l + n_s}. \tag{10}$$

The values of activities in solution were determined using the correlations of Tang *et al.*[54] and Tang and Munkelwitz.[55] In cases where there is insufficient water to dissolve all of the salt present, the minimum free energy was attained at a state corresponding to a layer of saturated solution in contact with a residual crystalline slab. In cases where there is sufficient or excess water, the minimum free energy corresponded to the most dilute solution. No regions with multiple equilibria are predicted for the macroscopic slab scenario and equilibrium is controlled solely by chemical potential. Figure 2 shows the free energy change for the most stable state as a function of water mole fraction in the simulation cell. Although the absolute value of ΔG^{dis} sharply increases beyond $x_{\mathrm{H_2O}} \approx 0.9$ (which corresponds to the solubility limit), values are negative even in cases with insufficient water for complete dissolution. Thus bulk thermodynamics predicts that dissolution will occur for the range of compositions in our simulation cell.

IV. RESULTS AND DISCUSSION

Simulations were performed at three different temperatures of 300, 350, and 400 K. The pressure was set equal to $1.013\,25 \times 10^5$ Pa (1 atm) at the lower two temperatures and elevated to 2.5 atm at 400 K to ensure a liquid phase for the water. The structure of the solid and liquid phases are characterized by radial distribution functions (RDFs) defined as

$$g(r) = \frac{1}{nN} \sum_i \sum_j \langle \delta[r - r_{ij}] \rangle, \tag{11}$$

where N is the total number of atoms, n is the number density, and r_{ij} is the separation between the atom pair specified by ij. For our system the Na–Na, Na–O, and O–O radial distribution functions are sufficient to fully characterize the system because the locations of all chloride ions are directly correlated to sodium ions in the lattice arrangement and the locations of all hydrogen atoms are directly correlated to oxygen atoms since the potentials used treat the water molecule as a rigid body.

The three sets of RDFs obtained at 300 K are shown in Fig. 3, varying with increasing void fraction. There is a minor change in the RDFs with void fractions within the two ranges of 0%–15% and 20%–40% and a distinct change of peak structure between the two sets of curves. This change is significant in the Na–Na and Na–O RDFs, both in shape and magnitude, and minor for the O–O RDF. The Na–Na RDF with void fraction ranging between 0% and 15% corresponds to an ordered crystalline phase with a long-range structure. Above 20%, however, the RDF corresponds to a disordered liquidlike phase, with the ions arranged such that there is a single peak corresponding to the nearest neighbor location, and no long-range order. The Na–O RDF above 20% shows a much larger peak at the nearest neighbor distance, indicating a greater degree of mixing between the ions and liquid water molecules. The O–O RDF reproduces the structure of liquid water in both cases.

Figure 4 shows the Na–Na RDFs generated by simulating a crystalline NaCl slab in the absence of water at 300 K. There are again two different morphologies corresponding to

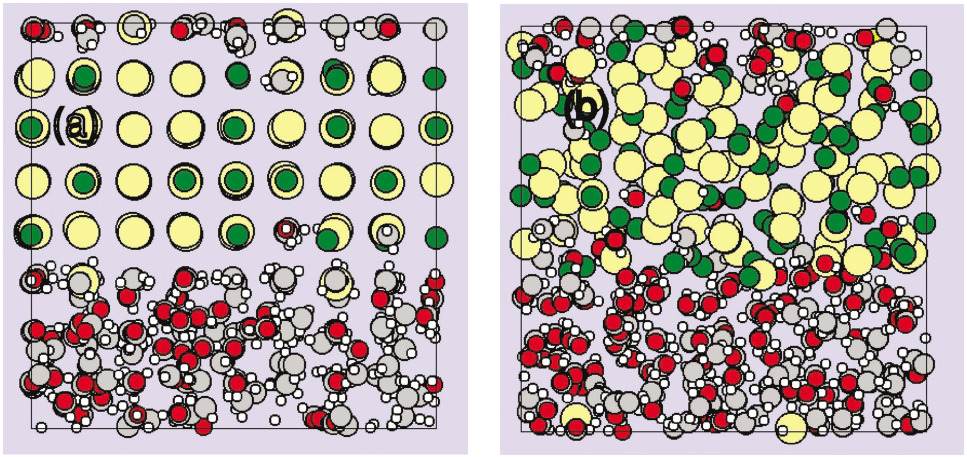

FIG. 5. (Color) Visual representation of post-run simulation cells at 300 K and 6 ns. (a) shows the post-run cell containing 10% voids, an example run containing fewer than the critical number of voids. There is limited interaction at the interface and no mixing. (b) shows the post-run cell containing 20% voids. This system contains more than the critical number of voids. Mixing of water molecules across the interface can be clearly observed.

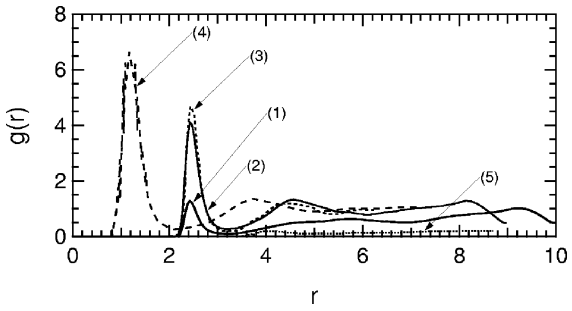

FIG. 6. Comparison of Na–O radial distribution functions. (1) Crystalline slab containing 20% voids, this work; (2) saturated solution at 300 K, this work; (3) 4.8*M* solution, Cavallari *et al.* (Ref. 56); (4) 4.5*M* solution, Chowdhuri and Chandra (Ref. 57); and (5) saturated solution, Zahn (Ref. 58). The RDFs have similar shapes but differ in the location and heights of the primary peak.

the ordered and disordered phases. The crystal structure is, on average, much clearer than the case with water, with sharper peaks around the lattice sites. The change from ordered to disordered phases occurs at a void fraction of 30%, which corresponds to the physical stability limit of the crystal. This value can be compared to the lower value of 15% when water is included in the simulation. The reduction in the void fraction at which RDFs change to the disordered type indicates that the water plays an important role in determining the arrangement of molecules in the dissolved or disordered phases indicating the physically distinct process of dissolution.

Additionally, visual examination of the simulation cells at the end of a run shows mixing of NaCl and water molecules across the interface above the critical void fraction, while there is no indication of such mixing for simulation cells below the critical void fraction. Figure 5 shows two such examples. The combination of these two factors leads to the conclusion that introduction of a critical number of voids in the crystal structure initiates dissolution.

A simple calculation using Fick's law of diffusion indicates that in a sodium chloride-water system complete dissolution would occur at a time scale of the order of 10 μs. At present, simulations of this time scale are not possible due to limited computational capacity. If computational resources were available, complete dissolution should be observable via this technique, using either extremely long simulation times with supercomputer resources or accelerated simulations at high temperatures.

It is interesting to compare the Na–O RDF obtained above the critical void fraction with the similar function obtained by direct simulation of a saturated sodium chloride solution. This comparison is shown in Fig. 6, which also contains RDFs available in literature.[56–58] The RDFs available in literature have identical shapes, but show a poor agreement in terms of location of the first peak (first solvation shell) and the heights of the peaks. The RDF obtained from a crystal-water cell in this work matches well with both the solution RDFs shown by Cavallari *et al.*[56] and the RDFs we obtained by simulating saturated solutions. The shape is identical to that of Chowdhuri and Chandra,[57] although the location of the first solvation shell is different. Simulations of NaCl-water slabs in contact that contain the requisite number of voids have at least the same macroscopic morphology as saturated NaCl solutions. There are no experimental data available on NaCl solution structure; however, such observations should be possible by neutron diffraction analysis.[59]

V. SENSITIVITY STUDIES

In this section we examine the sensitivity of void-induced dissolution to total system temperature, length of simulations, water potential model, and the location of the voids, as defined in Eqs. (3) and (4). The simulation cell and basic technique remain, as described previously.

Figure 7 shows the Na–Na RDFs at 350 and 400 K. A change in morphology and two distinct families of curves are observed, similar to the results obtained at 300 K. The Na–O and O–O RDFs have not been plotted at these temperatures, but show the same change in structure. Increasing the temperature decreases the critical void fraction. At 400 K the 15% curve clearly corresponds to the disordered phase, while at 350 K it shows characteristics from both families. The critical void fraction for the lowest temperature of 300 K is between 15% and 20%. This result is as expected, since simulations at higher temperatures correspond to higher molecular velocities, and the probability of atoms leaving their crystal lattice sites and dissolving in the water layer is higher. The disordering of crystals in the absence of water is much less sensitive and continues to occur around 30% even at the

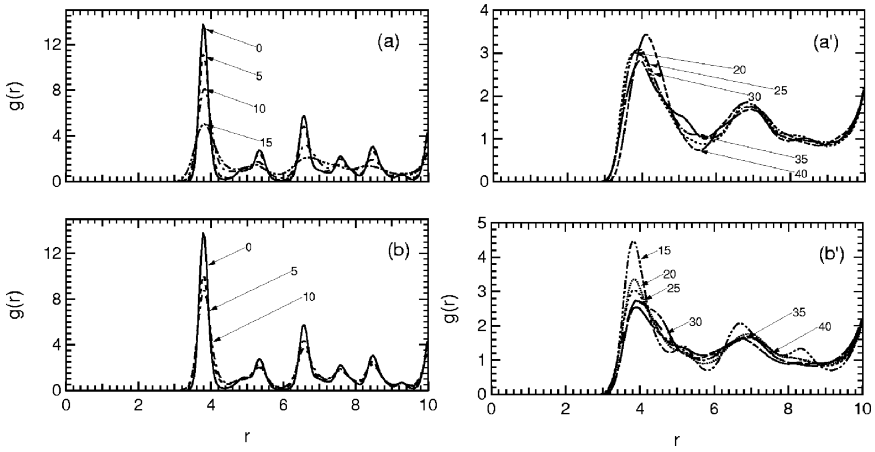

FIG. 7. Comparison of the ordered and disordered Na–Na RDF families at higher temperatures. (a) and (a′) are at 350 K and (b) and (b′) are at 400 K. The curves are labeled identically to Fig. 3. A lower void content induces change between the families at higher temperatures.

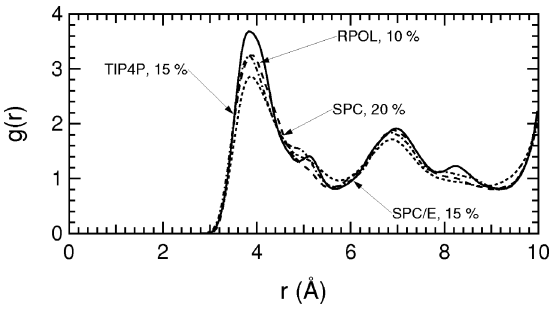

FIG. 8. Comparison of Na–Na RDFs obtained using different water models, above the critical void fraction required for dissolution. The model used and the corresponding critical void fraction required are indicated using tags. The Na–Na RDFs for the undissolved cases are identical, overlap, and not plotted. The dissolved RDFs are similar, with minor variations associated with the various descriptions of the water molecules.

elevated temperatures. There is an even clearer distinction between the dissolution and melting-like phenomenon at elevated temperatures.

Figure 8 shows the variation of the Na–Na RDF due to the models for water potential described in Sec. II. Qualitatively, the results do not change. At low void fractions, there is limited interaction between the NaCl and water molecules, and the RDFs are of the undissolved type. As voids are introduced into the NaCl structure, the RDFs change to the dissolved type above a critical value. Quantitavely, the void fraction at which this change takes place differs between the models. The simplest SPC model, which does not account for polarizability, requires the maximum addition of voids, at 20%. The RPOL model, which explicitly calculates the polarizability as a function of the ionic neighborhood of the water molecules, requires the least amount of voids, at 10%. The TIP4P and SPC/E models, which both approximate the polar nature of the water molecule by the imposition of fixed partial charges on the atoms, require the addition of an intermediate amount of voids. These results show that fewer voids are required when interactions between the ionic charges and the water dipole are allowed to be stronger. Our technique for identifying dissolution is independent of the exact description of the water molecule used. Though the RPOL model which contains an explicit polarizability term requires the least defects in the NaCl crystal for observable dissolution, the compulational price for using the complex model is high. Therefore, we have determined that the TIP4P and SPC/E models are satisfactory models for this application.

The effect of the location of voids in the crystal slab is indicated in Figs. 9 and 10. We label voids located at lattice sites not adjacent to the water layer as interior voids, and voids located adjacent to the water layer as surface voids. Figure 9 shows that the effect of the distribution is small, but simulation cells which have an even or balanced distribution between surface and volume voids show a greater tendency towards the disordered state than cells which have either kind of void exclusively. The impact of varying ϕ' as defined in Eq. (4) is more pronounced. Simulation cells with higher values of ϕ' show a greater tendency toward dissolution. The singular case with a low volume void fraction and a low value of $\phi'=0.077$ shown in Figs. 10(a) and 10(a′) show morphology closer to the ordered crystalline phase. We can conclude that the best conditions for observing dissolution occur when the total voids are balanced between surface and volume regions, and also have a high void distribution function, i.e., many small voids rather than a few big voids.

The time evolution of dissolution can be observed in Fig. 11. Although the time scale required for complete dissolution (10 μs) is at present unrealistic, we varied simulation lengths from 1 to 300 ps. The length of time step was changed to keep the total number of steps constant. A short run using a time step of 0.01 fs for 1000 steps serves as "zero-time" run, for comparison. It appears that the change in average system structure from undissolved to dissolved occurs at very short time scales, and then asymptotically approaches the final equilibrium value. This evolution can easily be observed from the first peak in each RDF. The change between 1 and 300 ns is most pronounced in the Na–Na and Na–O functions, and minor in the O–O function. This is expected, since we observed a major change in the morphologies of the Na–Na and Na–O RDFs, and only a minor change in the O–O RDF.

VI. CONCLUSIONS

Classical molecular dynamics simulations of the NaCl/water interface were carried out at various conditions. They show that although bulk thermodynamics indicates that dis-

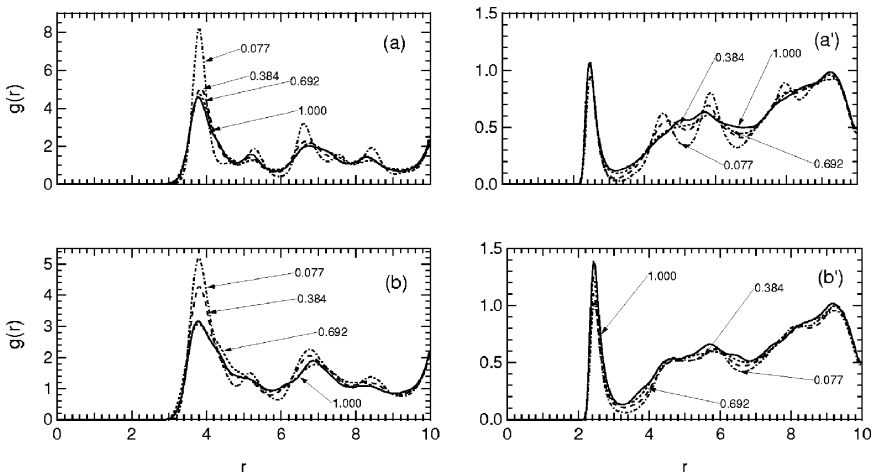

FIG. 9. Comparison of Na–Na RDFs with varying volume and surface void distributions at 300 K. The tags on various lines show void fraction present on the surface. (a) Total void 15%. The simulation with 5% void on the surface has characteristics very similar to solution, and 0% void on the surface is least similar to solution. (b) Total void 20%. The simulation with 15% void on the surface is most similar to solution, and the cases with 0% and 20% on the surface are least similar.

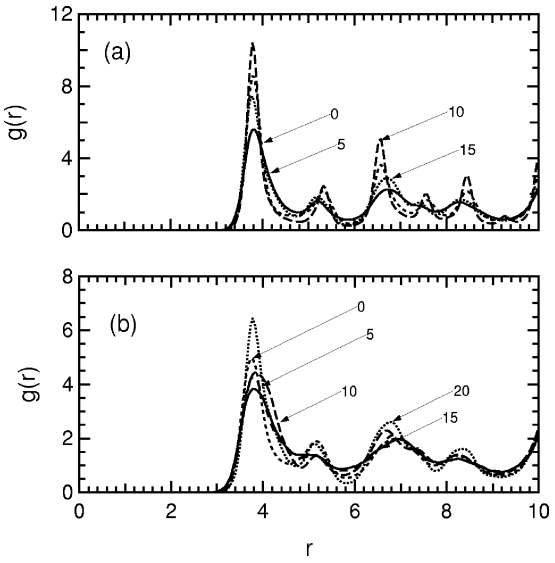

FIG. 10. Comparison of Na–Na and Na–O RDFs with varying void distribution function ϕ' on the surface. (a) and (b) show Na–Na RDFs, and (a′) and (b′) show Na–O. (a) and (a′) have a total void content of 15%, of which 10% is located on the surface. The case with the lowest ϕ' appears more crystalline than disordered. All others show disordered behavior. (b) and (b′) have a total void content 20%, of which 10% is on the surface. All values of ϕ' result in disordered behavior, with larger values corresponding to larger deviation from the ordered structure.

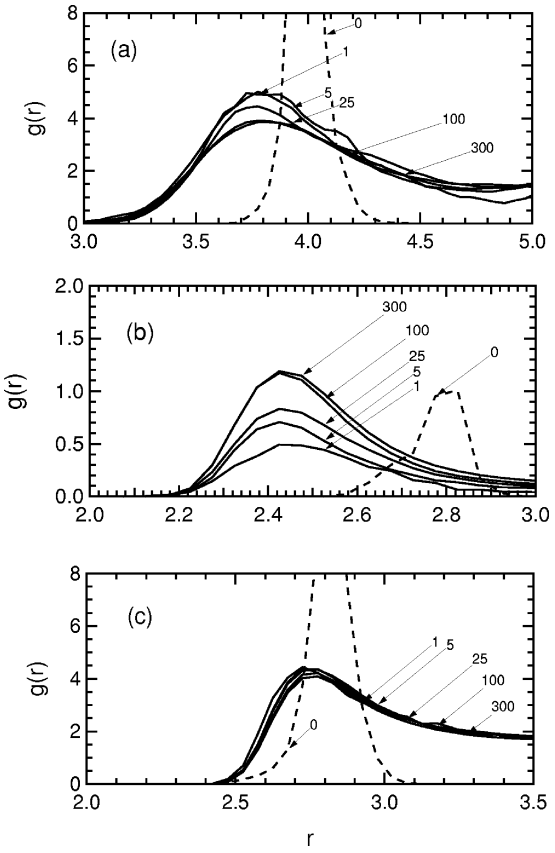

FIG. 11. Time evolution of the (a) Na–Na, (b) Na–O (c), and O–O RDFs, for a simulation cell containing 20% voids at 300 K, which is expect to dissolve. The solid lines are RDFs obtained from simulation runs of varying lengths and are tagged with time in picoseconds. The dashed lines are obtained from a run of 0.01 ps and indicate our zero-time structures.

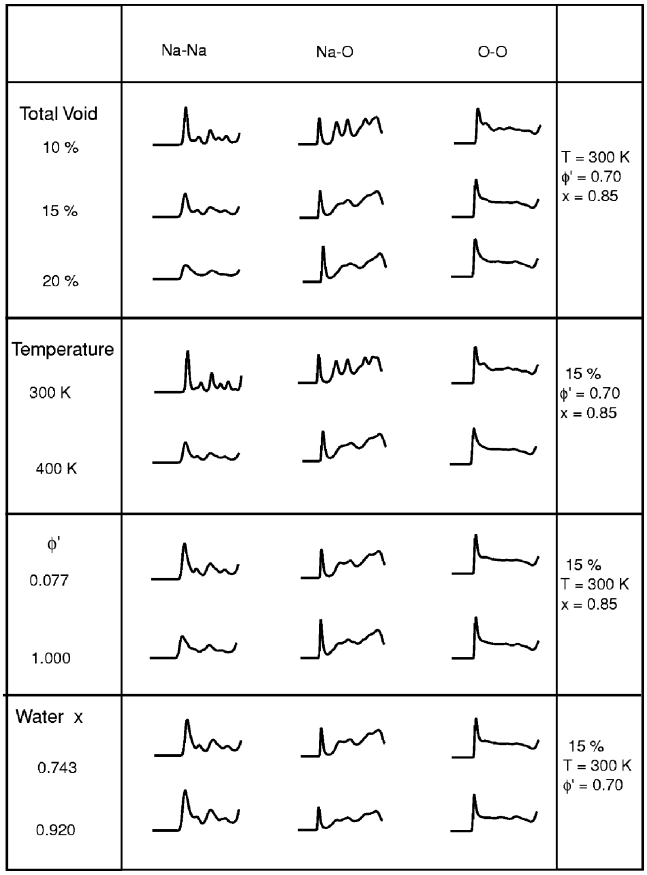

FIG. 12. Summary of RDFs demonstrating the transition between dissolved and undissolved system structures as a result of introducing voids. Holding all physical conditions constant, the RDFs. transition from an undissolved structure at 10% void to a dissolved structure at 20% void. The sensitivities of the technique to temperature, void distribution, and total water are also shown. All RDFs are sketched between 0 and 10 Å radial distance and have the same y axes within each set.

solution of the NaCl should occur in the water layer at all composition ratios, dissolution will not occur without lattice defects. This behavior may be a kinetic limitation of the simulation technique and geometry used that agrees with earlier work.[20] The introduction of lattice defects in the form of voids on both the crystalline surface and in the volume leads to an initiation of the process of dissolution. The total number of voids required is reasonable and consistent with measured physical properties of naturally occurring NaCl crystals, which contain volume defects and cleave to form stepped surfaces.

The effect of introduction of voids into the simulation lattice is summarized in Fig. 12. There are clearly two families of curves, which for the Na–Na RDFs are the sharply peaked crystalline or undissolved structure, and smoother or dissolved structure, with a primary peak for nearest neighbors and insignificant long-range order. The Na–O and O–O RDFs similarly break down into two distinct families. The introduction of approximately 20% voids into the NaCl structure is sufficient to initiate dissolution at room temperatures. Increasing the temperature to 400 K reduces the number of voids required to 15%. Simulation cells where the voids are equally split between surface and volume, and highly distributed across the surface ($\phi'=1$) dissolve at

lower void fractions. There is little observable effect of introducing excess water into the simulation cell.

The technique of introducing voids provides a useful MD tool, which not only provides a better physical representation of the system being simulated but also provides the first MD simulation of dissolution. Although time scales required to observe dissolution of a bulk crystalline phase remain too large for complete, detailed molecular simulations, this work provides a methodology which in combination with accelerating algorithms and superior computational power may result in successful MD simulation of the dissolution process.

ACKNOWLEDGMENTS

This material is based upon work supported by the National Science Foundation under Grant No. 0304213. Any opinions, findings, conclusions, and recommendations are those of the authors and do not necessarily reflect the views of the National Science Foundation. The authors thank J. Andrew McCammon, Jeremy Kua, George Biskos, and Matthew Wise for their many helpful suggestions.

[1] L. M. Russell and Y. Ming, J. Chem. Phys. **116**, 311 (2002).
[2] A. Singewald and L. Ernst, Z. Phys. Chem., Neue Folge **124**, 223 (1981).
[3] S. T. Martin, Chem. Rev. (Washington, D.C.) **100**, 3403 (2000).
[4] B. J. Finlayson-Pitts and J. C. Hemminger, J. Phys. Chem. A **104**, 11463 (2000).
[5] B. J. Finlayson-Pitts, Chem. Rev. (Washington, D.C.) **103**, 4801 (2003).
[6] R. C. Hoffman, M. A. Kaleuati, and B. J. Finlayson-Pitts, J. Phys. Chem. A **107**, 7818 (2003).
[7] R. C. Hoffman, A. Laskin, and B. J. Finlayson-Pitts, J. Aerosol Sci. **35**, 869 (2004).
[8] W. C. Keene, D. J. Jacob, A. A. P. Pszenny, R. A. Duce, J. J. Schultztokos, and J. N. Galloway, J. Geophys. Res., [Atmos] **98**, 9047 (1993).
[9] W. C. Keene and A. A. P. Pszenny, Science **303**, 628 (2004).
[10] M. P. Allen and D. J. Tildesley, *Computer Simulation of Liquids* (Oxford University Press, Oxford, 1987).
[11] M. P. Allen and D. J. Tildesley, *Computer Simulation of Liquids* (Clarendon, Oxford, 1987).
[12] J. Anwar, D. Frenkel, and M. G. Noro, J. Chem. Phys. **118**, 728 (2003).
[13] H. Ohtaki and T. Radnal, Chem. Rev. (Washington, D.C.) **93**, 1157 (1993).
[14] A. P. Lyubartsev and A. Laaksonen, J. Phys. Chem. **100**, 16410 (1996).
[15] S. Koneshan and J. C. Rasaiah, J. Chem. Phys. **113**, 8125 (2000).
[16] P. Jungwirth and D. J. Tobias, J. Phys. Chem. B **105**, 10468 (2001).
[17] M. Lisal, W. R. Smith, and J. Kolafa, J. Phys. Chem. B **109**, 12956 (2005).
[18] L. Perera and M. L. Berkowitz, J. Chem. Phys. **95**, 1954 (1991).
[19] P. Jungwirth and D. J. Tobias, J. Phys. Chem. A **106**, 379 (2002).
[20] H. Shinto, T. Sakakibara, and K. Higashitani, J. Phys. Chem. B **102**, 1974 (1998).
[21] H. Shinto, T. Sakakibara, and K. Higashitani, J. Chem. Eng. Jpn. **31**, 771 (1998).
[22] E. Oyen and R. Hentschke, Langmuir **18**, 547 (2002).
[23] S. Piana and J. D. Gale, J. Am. Chem. Soc. **127**, 1975 (2005).
[24] S. Kerisit, S. C. Parker, and J. H. Harding, J. Phys. Chem. B **107**, 7676 (2003).
[25] S. Kerisit and S. C. Parker, J. Am. Chem. Soc. **126**, 10152 (2004).
[26] R. Kristensen, S. L. S. Stipp, and K. Refson, J. Chem. Phys. **121**, 8512 (2004).
[27] O. W. Duckworth and S. T. Martin, Am. Mineral. **89**, 554 (2004).
[28] O. W. Duckworth, R. T. Cygan, and S. T. Martin, Langmuir **20**, 2938 (2004).
[29] S. Alavi and D. L. Thompson, J. Chem. Phys. **122**, 154704 (2005).
[30] S. Alavi and D. L. Thompson, J. Phys. Chem. B **109**, 18127 (2005).
[31] L. Huggins and J. E. Mayer, J. Chem. Phys. **1**, 643 (1933).
[32] H. J. C. Berendsen, J. P. M. Postma, W. F. van Gunsteren, and J. Hermans, *Intermolecular Forces* (Reidel, Dordrecht, 1981).
[33] H. J. C. Berendsen, J. R. Grigera, and T. P. Straatsma, J. Phys. Chem. **91**, 6269 (1987).
[34] W. L. Jorgensen, J. Chandrasekhar, J. D. Madura, R. W. Impey, and M. L. Klein, J. Chem. Phys. **79**, 926 (1983).
[35] L. X. Dang, J. Chem. Phys. **97**, 2659 (1992).
[36] D. E. Smith and L. X. Dang, J. Chem. Phys. **100**, 3757 (1994).
[37] D. Frenkel and B. Smit, *Understanding Molecular Simulation* (Academic, New York, 2002).
[38] R. M. Lynden-Bell and J. C. Rasaiah, J. Chem. Phys. **107**, 1981 (1997).
[39] T. R. Forester and W. Smith, DLPOLY 2.14 (1995).
[40] P. M. Agrawal, B. M. Rice, and D. L. Thompson, J. Chem. Phys. **118**, 9680 (2003).
[41] P. M. Agrawal, B. M. Rice, and D. L. Thompson, J. Chem. Phys. **119**, 9617 (2003).
[42] G. F. Velardez, S. Alavi, and D. L. Thompson, J. Chem. Phys. **120**, 9151 (2004).
[43] G. F. Velardez, S. Alavi, and D. L. Thompson, J. Chem. Phys. **119**, 6698 (2003).
[44] S. Nosé, J. Chem. Phys. **81**, 511 (1984).
[45] W. G. Hoover, Phys. Rev. A **31**, 1695 (1985).
[46] D. Frenkel and B. Smit, *Understanding Molecular Simulation* (Academic, New York, 2000).
[47] D. C. Rappaport, *The Art of Molecular Dynamics Simulations* (Cambridge University Press, Cambridge, 1987).
[48] K. D. Gibson and H. A. Scheraga, J. Phys. Chem. **99**, 3752 (1995).
[49] H.-J. Weber, H.-L. Keller, C. Lathe, and C. Popa-Varga, J. Appl. Phys. **98**, 034317 (2005).
[50] L. E. Steiner, *Introduction to Chemical Thermodynamics* (McGraw-Hill, New York, 1941).
[51] A. W. Adamson, *Physical Chemistry of Surfaces* (Wiley, New York, 1990).
[52] A. A. Abramzon and R. D. Gauberk, Zh. Prikl. Khim. (S.-Peterburg) **66**, 1428 (1993).
[53] W. Wu and G. H. Nancollas, Adv. Colloid Interface Sci. **79**, 229 (1999).
[54] I. N. Tang, H. R. Munkelwitz, and N. Wang, J. Colloid Interface Sci. **114**, 906 (1986).
[55] I. N. Tang and H. R. Munkelwitz, Atmos. Environ. **27**, 467 (1994).
[56] M. Cavallari, C. Cavazzoni, and M. Ferrario, Mol. Phys. **102**, 959 (2004).
[57] S. Chowdhuri and A. Chandra, J. Chem. Phys. **115**, 3732 (2001).
[58] D. Zahn, Phys. Rev. Lett. **92**, 040801 (2004).
[59] R. H. Tromp, G. H. Neilson, and A. K. Soper, J. Chem. Phys. **96**, 8460 (1992).